IEEE Access
Multidisciplinary | Rapid Review | Open Access Journal

Received October 1, 2020, accepted October 25, 2020, date of publication November 10, 2020, date of current version November 30, 2020.

Digital Object Identifier 10.1109/ACCESS.2020.3037250

Proximal Actuation of an Elastically Loaded Scissors Mechanism for the Leg Design of a Quadruped Robot

MUHAMMAD HAMZA ASIF NIZAMI[1], (Member, IEEE), ZAID AHSAN SHAH[1], YASAR AYAZ[1], (Senior Member, IEEE), MUHAMMAD JAWAD KHAN[1], (Member, IEEE), SARA ALI[1], (Member, IEEE), MUHAMMAD NAVEED[1], (Member, IEEE), KHALID AKHTAR[1], DARREN DANCEY[2], AND RAHEEL NAWAZ[2,3], (Member, IEEE)

[1]School of Mechanical and Manufacturing Engineering, National University of Sciences and Technology, Islamabad 44000, Pakistan
[2]Department of Computing and Mathematics, Manchester Metropolitan University, Manchester M15 6BH, U.K.
[3]Department of Operations, Technology, Events and Hospitality Management, Manchester Metropolitan University, Manchester M15 6BH, U.K.

Corresponding author: Sara Ali (sarababer@smme.nust.edu.pk)

This work was supported by the National University of Sciences and Technology (NUST), Pakistan.

ABSTRACT Spring Loaded Pantographs (SLPs) are frequently used in designing lightweight limbs for multi-legged robots. Quadruped robots that incorporate cable-pulled SLP legs have proven to be agile, robust and capable of conserving energy during their gait cycle. In such designs, the extension of the distal segments via the knee joint is dependent upon the length of the cable. In this article we propose the use of an Elastically Loaded Scissors Mechanism (ELS Mechanism or ELSM), which is a variant of the SLP. Driven by 'pulling' onto the proximal joint of the scissors as opposed to the distal joint, this proposed leg utilizes the increased mechanical advantage of the scissors mechanism to 'amplify' input angles to larger output displacement by the knee joint. Analysis and Simulations reveal that the proposed mechanism achieves increased motion speed as compared to the SLP mechanism. This, however, comes at the cost of higher load on the actuator which serves as an engineering trade-off. This is validated by experimentation using motion capture and load motor techniques of the SLP and ELS configurations in a physical quadruped robot.

INDEX TERMS Robot locomotion, spring loaded pantograph, elastically loaded scissors mechanism, leg mechanism, robot design, compliant mechanisms.

I. INTRODUCTION

Legged locomotion is widely considered a prime candidate for handling uneven terrains since it requires comparatively sparse interaction with ground than its wheeled or tracked locomotion alternatives. Biological inspiration plays a vital role in our understanding of legged locomotion, e.g. [1], [2]. This gives rise to mathematical models of locomotion such as the Spring Mass System [3], the Linear Inverted Pendulum (LIPM) [4], The 3 Linear Pendulums (3LP) [5], Rimless Wheel (RW) [6] and many more [7]. Recently, several robots have been built on the basis of the above mentioned models of locomotion. From [8] who demonstrated the application of the Spring Mass model in the design of a family of dynamically stable robots ranging from single legged hoppers to quadruped robots, to the design of SCOUT II [9], BigDog [10], StarlETH [11] and ATRIAS [12], ATLAS and PETMAN [13] and other such dynamically stable robots.

These models govern the planning and control of most modern walking robots. The main aim is to either simplify or optimize the control strategy [14]–[16] or to robustly utilize the dynamics in a more convenient manner [17], [18] among other criterion [19].

Energy efficiency is an important hallmark of walking organisms in nature and can be realized in the design of compliant legs for walking robots [20]. Interestingly such robots can be designed to utilize their natural dynamics that differ from the traditional method of robot control [21] and [22]. It has been demonstrated in the past that these approaches result in robust locomotion even when there is limited, indirect or no terrain information [23] and [24].

Based on the idea of implicit or no ground force sensing, a certain level of robustness and stability in walking robots can still be achieved through Central Pattern

The associate editor coordinating the review of this manuscript and approving it for publication was Hamid Mohammad-Sedighi.

Generators (CPGs) [25]. Inspired from the behavior exhibited by the motor neuron activations in humans and animals [26], CPGs cause motion in several different types of living organisms [27]. Recently, several robots have been developed that depend on central pattern generators for stable locomotion [28] and [29].

The extent to which different control strategies can be implemented depends on the nature of the leg itself. In particular, the leg mechanism and the actuation technique play a vital role in this regard [30]. A biologically inspired method of leg actuation is by the usage of a mechanism called Spring Loaded Pantographs (SLPs). The intuition behind the usage of pantographs is bio-inspired as studies have indicated that mammals mostly tend to keep the proximal and distal segments parallel during the gait cycle [31]. Sprowitz et. al. demonstrated the application of Advanced Spring Loaded Pantograph (ASLP), a variant of the SLP, in Cheetah-Cub [32] and Oncilla Robots [41] as they achieved dynamic trot gait. Although, it is possible to achieve the same parallel-angle behavior by using actuated pin knee joints, but that would add a further layer of control complexity that can otherwise be removed by using the SLP approach. One of the advantages of the SLP mechanism is that it makes it possible to actuate the leg via a cable which enables the actuators to be mounted onto the body and hence reducing the leg mass and inertia properties. Secondly, during stance stage, when the leg is in contact with the ground, the cable 'sags', bypassing the actuator and making the load in series with spring. This makes the actuator decoupled from the dynamics of the legged robot and dependent upon the energy stored in the spring.

One feature of the cable-pulled SLP mechanism is that length of the thread required to actuate the knee joint is rolled onto a pulley whose diameter is directly proportional to the length of the rolled cable. This means that in order to significantly retract the knee joint, a larger diameter pulley is required, otherwise the reach of the leg, and hence its ability to traverse uneven terrains and to reject disturbances from the ground is compromised. This would further affect the weight as the robot is scaled up for larger practical applications.

The efficiency in terms of output motion of the SLP mechanism can be improved by replacing the pantographic mechanism with a scissors mechanism. Therefore, we propose a variant of the SLP mechanism, the Elastically Loaded Scissors Mechanism (ELSM or ELS Mechanism) because of its high mechanical advantage, compact design and parallel segment property as seen in Fig. 1. The role of scissors mechanisms as transmission systems has been previously explored in [33] and [34]. Incorporating it gives the bio-inspired leg design certain desirable properties as will be discussed in the following sections.

The proposed mechanism does not affect the overall power transmission, it just varies the torque velocity ratio. Another advantage of scissors transmission over traditional gear transmissions is that it does not get affected by backlash. Furthermore the proposed ELS mechanism requires less thread to

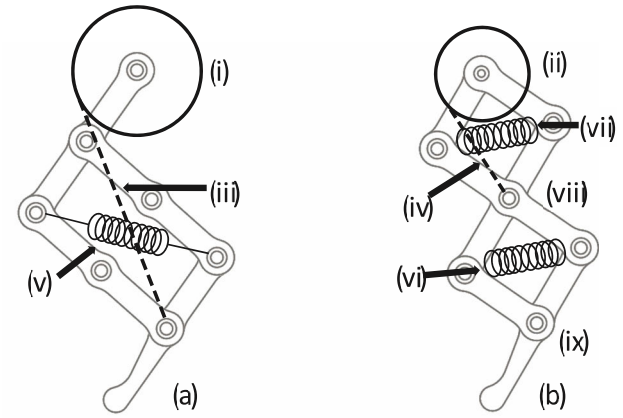

FIGURE 1. The Spring Loaded Pantograph (a) and Elastically Loaded Scissors (b) configurations considered. (i) and (ii) are pulleys, (iii) and (iv) represent the cable threads, (v), (vi) and (vii) represent elastic elements, (viii) represents the proximal joint and (ix) represents the distal joint.

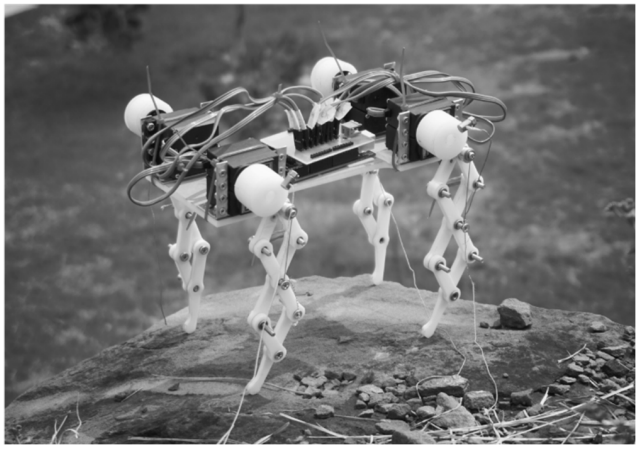

FIGURE 2. Felis - A Planar Reconfigurable Quadruped Robot.

be rolled onto the actuator pulley as compared to the SLP mechanism for the same amount of knee joint retraction (high mechanical advantage). If servo motors are used, as was done in the EPFL cheetah robot [32], [42], the rotational velocity saturates at a certain threshold value. Using the mechanical advantage of the scissors mechanism higher output range of motion is attainable for lower input range of motion. This enables us to 'harvest' higher step down velocities of the foot as compared to the SLP design.

It should be noted that if the same behavior is to be expected from a robotic leg with individually geared joints, a clutching mechanism would need to be developed to ensure that the leg operates in a parallel elastic configuration. This would mean that once the foot contacts the ground the actuators should decouple and the pose retention becomes dependent on the elastic elements inside the leg. This is a comparatively unfeasible arrangement and the clutching mechanism will add undesirable weight to the robot. Alternatively, stiffness control through other means can also be achieved [35], [36] and [37].

It should also be noted that although Scissor Mechanisms have been utilized previously for a hydraulic legged robot Baby-Elephant [38]. However, application of this mechanism has been restricted to payload carrying robots which are not meant for agile dynamic locomotion. Whereas, the aim of this article is to propose a lightweight ELS leg, with proximal actuation and compliance for energy storage.

A. RESEARCH CONTRIBUTIONS

In this research a novel leg mechanism is introduced that is actuated through a servo-tendon technique, reducing the leg weight and hip torque. The leg mechanism can be retracted by pulling onto the proximal joint of the linkage as compared to traditional SLP mechanisms and hence results in faster knee retraction than traditional SLP mechanisms. This increases the stepping speed of the mechanism and is particularly useful in cases where high stepping frequencies cannot be attained due to actuator saturation. Simulations are performed to demonstrate the effectiveness of the technique and experiments are performed to verify the results and to gauge the performance of the mechanism.

II. MECHANICAL MODELING

This section discusses the design intent and the kinematics of the proposed ELS leg mechanism.

A. DESIGN INTENT AND ACTUATION STRATEGY

The aim of the research conducted regarding the design of the ELS leg is basically, the design of a lightweight leg for agile quadruped locomotion. The lightweight design was achieved by placing the actuators driving the legs in the torso segment of the robot. As most common leg designs incorporate a minimum of two degrees of freedom (DOF), the leg design had to incorporate two actuators. The hip/shoulder joints would be directly driven whereas the knee/elbow joints would be driven by a cable. In order to restore the knee/elbow joint to their zero-loading configuration, an elastic element would be used, we propose the usage of rubber bands, as experimentation carried out on them show acceptable deviation from linearity within the loading range of the ELS leg.

As it had been pointed out that in small sized quadrupeds, the major hindrance to achieve bio-inspired locomotion is the inability of servo motors actuating the knee joint to reach beyond their saturation velocity to achieve higher stepping frequency, we propose the usage of scissors mechanisms instead of pantograph mechanism. This we prove will increase the stepping frequency due to the higher mechanical advantage of the scissors mechanism.

We would also like to prove that, although the proposed method demands higher torque from the knee actuators, this does not adversely affect robot's performance. The discussion is as follows: The maximum work done by the knee actuator is only during the flight stage when the servo motor is driven to store energy in the spring and retract the leg. Therefore, the weight of the robot will not act as load on the knee servo. The only other concern is the effect of dynamic effects that may cause loading on the actuators which can be ignored on the basis of lightweight-legs assumption in conjunction with the spring-mass model.

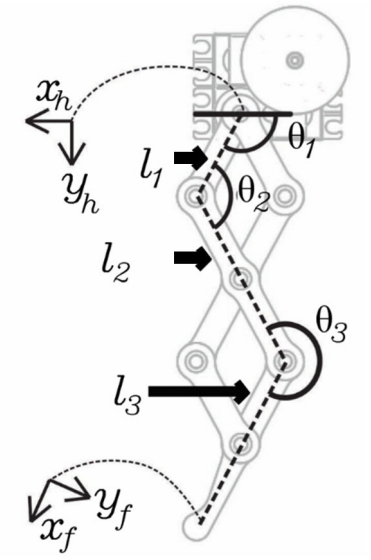

FIGURE 3. Frame assignment and parameters.

B. KINEMATICS

Using Denavit-Hartenberg parameters to solve the kinematics of a parallel mechanism is a bit tricky. To solve this problem, effective length segments resembling a three segment leg were chosen as shown in Fig. 3, thus measuring the kinematics in terms of simple 3-link parallel manipulator. Where angles θ_1, θ_2 and θ_3 represent joint-space positions. Note that as the angles θ_1 and θ_2 are the only independent variables, as $\theta_3 = 2\pi - \theta_2$ due to the scissors mechanism.

$$x = l_2 \cos(\theta_1 + \theta_2) - (l_1 + l_3)\cos(\theta_1) \tag{1}$$

$$y = (l_1 + l_3)\sin(\theta_1) - l_2 \sin(\theta_1 + \theta_2) \tag{2}$$

$$\varphi = \theta_1 \tag{3}$$

where x and y represent the cartesian-space position of the foot frame with respect the shoulder frame, and φ is the angle between the hip frame and the foot frame. The motion of the foot frame with respect to the hip frame as the joint angles are varied yields highly non-linear motion.

Solving analytically, the inverse kinematics of the leg yields the following results:

$$\theta_1 = \varphi \tag{4}$$

$$\theta_2 = \arctan\left[\frac{y-(l_1+l_3)\sin(\theta_1)}{l_2}, \frac{x-(l_1+l_3)\cos(\theta_1)}{l_2}\right] - \theta_1 \tag{5}$$

$$\theta_3 = 2\pi - \theta_2 \tag{6}$$

For a complete derivation refer to appendix A. As it is evident from Eq. 4 that two solutions exist for θ_1. This indicates the two configurations in which it is possible for the foot to

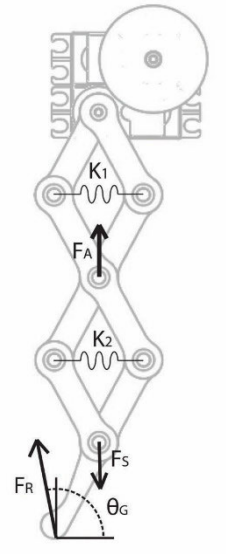

FIGURE 4. External forces acting on the leg.

achieve the requisite Cartesian position, and thus by ensuring maximum and minimum angular positions, these equations can be employed for calculating the Cartesian frame position of two coronal plane leg pairs.

As with all the legs with revolute joints, when the robot lifts the leg, the joints move by reducing the vertical distance between the hip/shoulder and the foot, however, the outer vertices, or 'knees', of the mechanism begin to occupy more horizontal space. If a leg with significantly articulated knee joints is rotated, the knee may come in contact with the ground before the foot. While stepping in narrow or inclined surfaces, this presents the undesired collision may grossly affect the robot's predicted states. Hypothetically, if the leg is fully collapsed, the maximum horizontal space obstruction possible by the proposed ELS mechanism is equal to the end effector position for the case of a fully collapsed leg, that is, at $\theta_1 = \pi$ rad and $\theta_2 = \theta_3 = 0$ rad, the forward kinematics equations above yields the obstruction to occupy a horizontal space equal to l_1. It can be easily seen by using the kinematic equations of SLP constrained by the same maximum leg extension and joint values as the ELS mechanisms that the maximum horizontal space occupied based on similar joint angle values, comes out to be twice as much as l_1. By this comparison, it is more feasible to use ELS mechanism for stepping on narrow or concave terrain profiles as well as for walking on inclined surfaces.

Another thing to notice in the inverse kinematics equation is the great degree of non-linearity (Fig.s 5 and 6). An advantage of this approach is the fact that as during stance θ_2 is dependent upon FG the system would not yet be uncontrollable, oscillations of the system can be still be controlled by the θ_1 and hence compensate for the losses that make it a damped system. Thus making it suitable for the Spring-Mass model. A detailed study of the system's frequency response is reserved for future work and is deemed beyond the scope of this research.

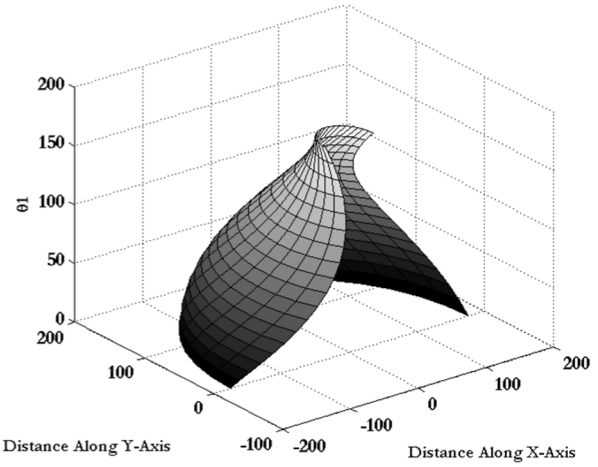

FIGURE 5. Variation of workspace in the XY-plane for various values of θ_1.

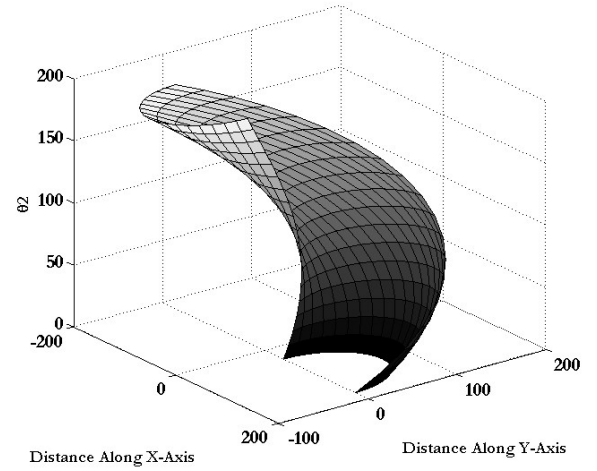

FIGURE 6. Variation of workspace in the XY-plane for various values of $\theta 2$.

C. ELASTIC ELEMENTS

Elastic elements are configured as shown in Fig. 4. The difference between F_A and F_S determines motion of the foot whilst the foot is in flight phase. F_R is the ground reaction force and θ_G is the angle of F_R as seen from a frame attached to the location of footstep placement. If the angle of attack of the foot varies, this will affect the angle between the foot frame and the ground frame and hence and hence effect the effect that the ground reaction force has on collapsing the leg.

To reduce the weight of the leg, rubber-bands were chosen, because of their good restoring force to weight ratio. O band (by Kyowa Limited Japan) rubber bands were chosen for this task and the average deflection under the action of loading due to added weights of a sample of 7 randomly chosen rubber-bands was plotted (Fig. 7).

We propose two scenarios under which loading of the elastic elements can occur: knee joint retraction in flight phase of the gait cycle and leg collapsibility under the action of loading during stance. An equation regarding the equiv-

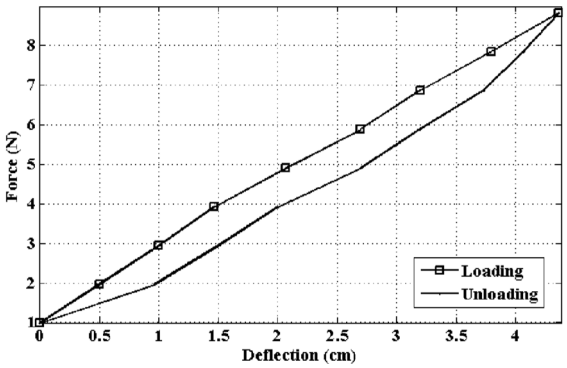

FIGURE 7. The Average Force-Deflection Data of O band Elastic Rubber bands measured in N-cm. On average it is assumed to be approx. 0.6 N-cm. Multiple rubber bands may be used to achieve desired stiffness.

alent leg stiffness under both types of loading is therefore needed.

Disregarding the retarding forces of friction, this will still give us an insight into the type of dynamic behavior to expect from the legs.

In the flight stage, the only possible way to actuate with the knee joint other than premature environmental interaction is via the actuating cable. Hence the system can be represented effectively as a Parallel Elastic System with the Equivalent stiffness given as:

$$K_y = K_e \tan\left(\frac{\pi - \theta_2}{2}\right) \tag{7}$$

$$F_s = K_y\left(l_0 - l_1 cos\left(\frac{\pi - \theta_2}{2}\right)\right) \tag{8}$$

$$l_0 = \sqrt{(l_1)^2 - \left(\frac{l_f}{2}\right)^2} \tag{9}$$

where K_y is the effective stiffness of the equivalent parallel elastic system. lf represents free length of the elastic element, $_{lo}$ represents the corresponding component of along $l_1 \cos\left(\frac{\pi-\theta_2}{2}\right)$ is the restoring force of the leg, K_e is the equivalent spring stiffness given by $K_e = \sum_{i=1}^{n} K_i$ where n is the number of elastic elements. For the Felis Robot shown in Fig. 2 only n = 1 was found to provide sufficient leg stiffness. It should be noted here that it as spring stiffness acts in series about the same joint as indicated by the above equation, a variety of K_1 and K_2 can be arranged such that their equivalent stiffness is the same, having no effect on the overall equivalent stiffen-ss. However, due to friction and other non-linearities and performance deterioration due to fatigue loading in the extreme cases (for instance $K_1 = 0$, K_2=K_e or $K_2 = 0$, K_1=K_e), highly varying results were achieved. This is due to the difficulty posed by modeling such non-linear systems on a case-by case basis. Part of the modularity of the proposed mechanism is that if K_1 and K_2 are used they will act as if in a series combination (adding to give equivalent stiffness). Thus, the effect of exempting K_2 is theoretically trivial. In practice, structural effects may be observed but that is beyond the scope of the current study.

A more complicated case, however, is the loading due to ground contact during stance stage, as it also depends on the angle that ground reaction force F_R makes with reference to a ground frame. We make a couple of assumptions here.

Firstly, we assume that the slope of the ground about the point of contact is zero. Secondly we assume that the horizontal component of the ground reaction force, $F_R \cos(\theta_G)$ is balanced by the high ground friction. That is to say the coefficient of static friction between the ground plane and the foot is sufficiently high so that the horizontal ground reaction force can be represented by the friction force. These assumptions are made to simplify the analysis and are similar to the assumptions made by [39].

The foot of the robot is intentionally kept round so as to keep the vertical distance from the point of impact on the flat ground to the foot axis purely vertical in terms of the ground frame. Foam based padding can be added to increase the surface area for higher contact friction.

This, in conjunction with the high-friction assumption, allows us to simply translate the vertical component of FR to the foot frame and solve the dynamics of the last segment of the ELS mechanism to find out the effect of loading on the springs due to FR. The said equation is given as follows:

$$I_3\ddot{\theta_3} = \tau_R - \tau_S - \tau_G - \tau_N + \tau_A \tag{10}$$

where: $\boldsymbol{\tau_N}$, the moment due to contact forces with respect to other linkages is assumed constant at the instance of impact, $\boldsymbol{\tau_A}$ the actuating torque is assumed to be zero, $\boldsymbol{\tau_S}$ is the torque due to springs. $\boldsymbol{\tau_G}$ is the torque due to gravity, $\boldsymbol{\tau_R}$ is the torque due to ground reaction force. Furthermore:

$$\tau_R = l_3 F_R \cos(\theta_G) \sin\left(\frac{\pi}{4} - \theta_C\right) \tag{11}$$

$$\tau_S = \frac{l_3}{2} F_S \cos(\theta_P) \sin\left(\frac{\pi}{4} - \theta_C\right) + \frac{l_3}{2} F_S \sin(\theta_P) \sin(\theta_C) \tag{12}$$

$$\tau_G = \frac{l_3}{2} g \sin\left(\frac{\pi}{4} - \theta_C\right) \tag{13}$$

where g is the gravitational acceleration and I3 is the Inertia Tensor of the last segment, θ_C is the correction angle of the leg and is given by $\theta_1 + \theta_p$ where θ_p is pitching angle of the body and θ_G is the angle that F_R makes with respect to the ground. These forces can be seen in Fig. 8.

As it can be predicted from the above equations, the loading on the spring due to ground F_R is dependent upon an interesting parameter, θ_G which is the angle of attack of the foot on the ground. To understand this variation we take a very simple case of static equilibrium to find out the dependency of F_S on θ_G.

On the basis of the plots in Fig. 10, we hypothesize that the trajectory generation of the foot in future pattern generation

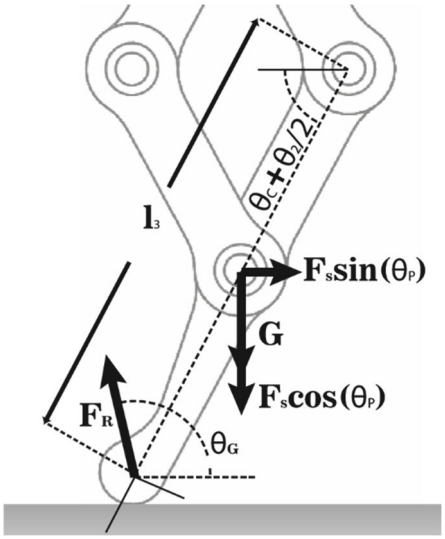

FIGURE 8. Ground reaction forces.

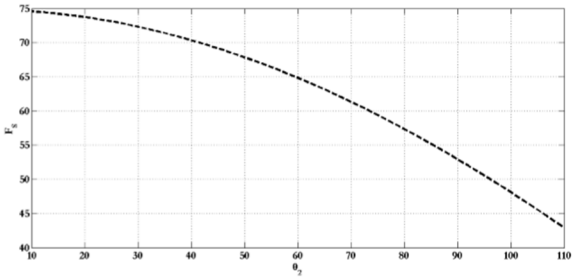

FIGURE 9. Variation trend of F_S with θ_2.

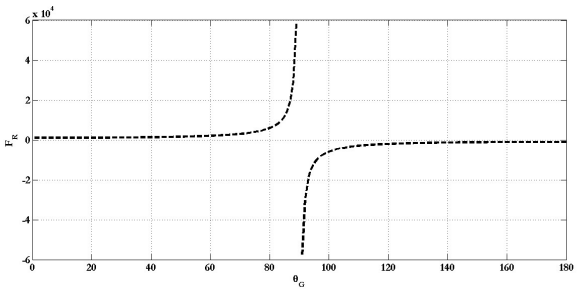

FIGURE 10. Variation trend of F_R in kgcm/s^2 Non-linear dynamics are evident with θ_G for Spring force: $F_S = 7.5$ N.

algorithms be kept so that the ground reaction force FR acts within a range of θ_G ranging from 80° to 100°.

As with SLP mechanism, the ELS mechanism depicts hybrid dynamic interactions. Any type of ground contact briefly decouples the knee actuators and the mechanism acts like a series mass spring system. Prior to ground touchdown, as the leg extends, the mechanism acts like a parallel elastic actuator. Therefore, when fully flexed, the springs store energy and when fully extended, the springs depend on ground reaction force for energy storage. Based on spring stiffness, the legs can be made strong in flexed state and by reducing the actuator's inertia and friction they can be made agile similar to the behavior of knee joints of traditional legged robots. Furthermore, the role of dynamic perturbations to achieve dynamic walking is planned to be explored in further studies and the development of controllers and appreciation of in depth dynamics is currently beyond the scope of this study.

TABLE 1. Salient Properties of the Felis Quadruped Robot.

Property	Value
Total weight (minus batteries)	1.01 kg
Leg weight (linkages and bearings)	130 grams
Maximum leg extension	16.3 cm
Minimum leg extension	6.3 cm
Robot height	21.4 cm
Robot width	16.7 cm
Robot length	22 cm
Leg material	Polymethyl-Methacrylate
Large pulley material	Nylon rod

III. MATERIALS AND DIMENSIONS

In the design of 'Felis' quadruped robot we have used acrylic (PolymethylMethacrylate) sheets that are also used in the making of medium plexiglass applications. This material offers a good strength-to-weight ratio having a compressive strength of upto 131 MPa and a tensile strength of upto 75.8 MPa for a density of 1.18 g/cm3. The main advantage of utilizing this material is due to the fact that it is very easy to cut it using laser cutting machinery which, when compared to milling or 3d printing, is a relatively inexpensive and fast method.

A CAD model of the Robot and the ELS leg was developed in SolidWorks can be seen in Fig. 11. The idea was to design a model that could be used to simulate results as well as be later used for manufacturing. Some salient features of the robot are discussed in Table 1.

A. SIMULATIONS

As was discussed earlier and shown in Fig. 11, a CAD model design of 'Felis' was made prior to fabrication. The choice of SolidWorks as the CAD software is based on the fact that the simulations of the robot could be tested in SolidMotion [43] which is based on ADAMS based physics engine. The following tests were carried out:

1) WORKSPACE AND TRAJECTORIES

Prior to being mounted, it is possible for two solutions and hence two configurations of the ELS leg as discussed earlier. It is interesting to know that if pattern generation using oscillators in the variables of actuator space are used, two unique gait patterns can be achieved in both of the mechanisms respectively. When planning in the workspace, the trajectories may be designed as desired within the workspaces of either of the two configurations. The workspace in configuration 1 is shown in Fig. 12, whereas the workspace

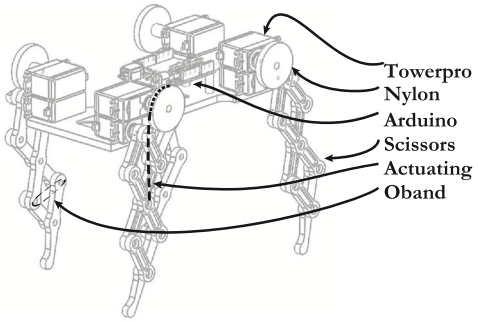

FIGURE 11. CAD model of Felis. The ELS mechanism of the legs was used in simulations.

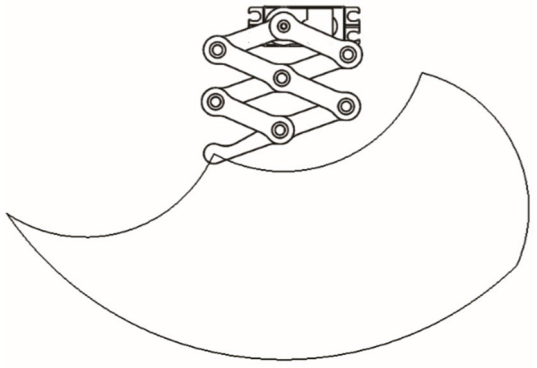

FIGURE 12. The workspace of the ELS Leg in configuration 1.

in configuration 2 is in Fig. 13. Notice how the second configuration seems to move the leg so as to strike the heel first on the ground, the contribution of this property in gait quality of a quadruped robot, however, is investigated in follow-up research on Felis Robot and is currently beyond the scope of this article. Although the servo motors used have an angular sweep of 180°, the designed range of motion which gives the workspaces is lesser than that as it delivers results which are not severely affected by joint friction.

Another important thing to notice is that all possible workspace states are holonomic in nature and are hence theoretically achievable by two degrees of freedom however, this case is not true for stance stage, where the workspace states may change depending on the ground reaction force FR.

2) PROXIMAL VS. DISTAL JOINT VELOCITY

Of the results obtained from the above simulation, we would be interested in knowing the velocity requirements for actuating the distal joint vs the proximal joint. We conclude from Fig. 14 that for the same workspace motion, the velocity required to actuate the distal joint becomes significantly higher than that required to move the proximal joint. Hence incorporation of proximal actuation in mechanisms will result in higher foot speeds and hence more agile locomotion.

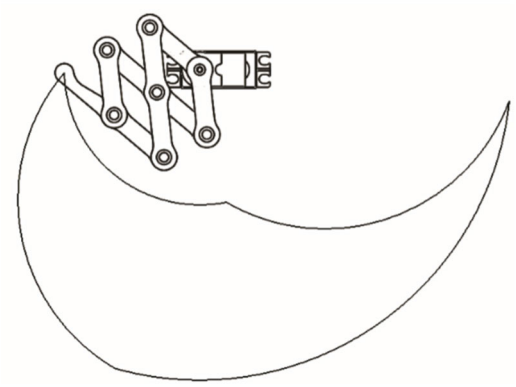

FIGURE 13. The workspace of the ELS Leg in configuration 2.

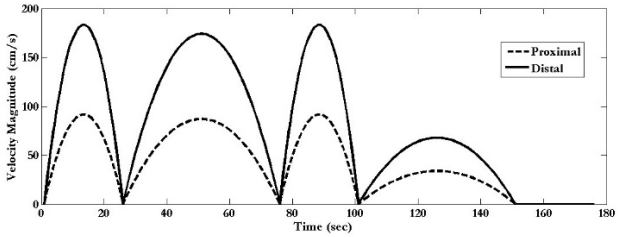

FIGURE 14. The Graphs plotting proximal vs. distal joint's linear velocity.

B. EXPERIMENTATION AND RESULTS

The design of Felis Robot allows the ability of reconfiguration. It is possible to achieve at least two configurations of closed mechanisms one of which is the proposed Elastically Loaded Scissors (ELS) configuration while the other is the Spring Loaded Pantograph (SLP) Configuration. Simulations have, in the previous chapters, proven the ability of the ELS configuration with proximal actuation to yield desirable properties of locomotion but how does this mechanism physically rank up against the SLP? This question is addressed by two experiments.

The first experiment tracks the motion of the two configurations while the second experiment compares the current consumed by them respectively.

In general, both leg configurations offer similar motion of the foot when it comes to the hip joint, however, the knee joint actuation differs highly and will be the subject of the following experimentation.

1) COMPARATIVE MOTION TRACKING EXPERIMENT

To validate the hypothesis made on the basis of simulations, we design and perform an experiment to measure and compare the velocity of the foot with SLP mechanisms.

Using the Felis Robot Platform, we design the two leg configuration models: SLP and ELS. We measure the displacement and velocity of the foot under the action of thread actuation, using motion capture open-source software Tracker [40] to track and log the foot displacement. For both cases, the same maximum and minimum

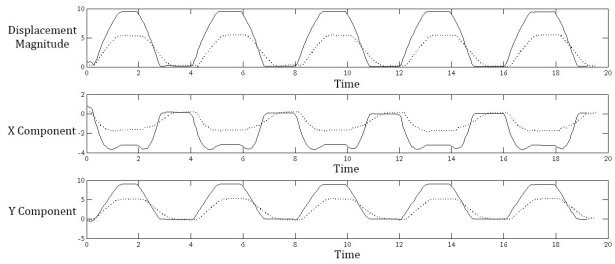

FIGURE 15. Displacement (cm) and its X and Y components. Solid lines represent ELS whereas dotted lines represent SLP.

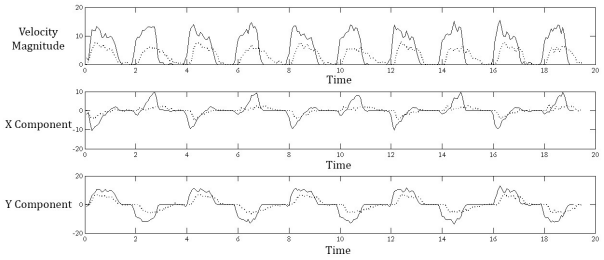

FIGURE 16. Velocity (cm/s) and its X and Y components. Solid lines represent ELS whereas dotted lines represent SLP.

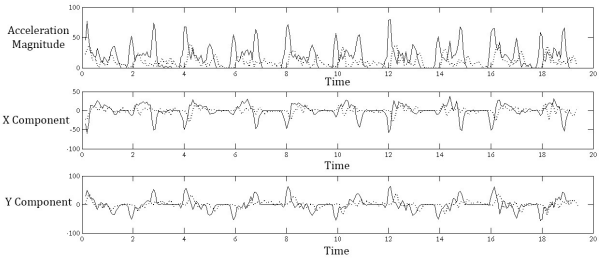

FIGURE 17. Acceleration (cm/s^2) and its X and Y components. Solid lines represent ELS whereas dotted lines represent SLP.

angular variations of $\theta 2$ controlled by the knee actuator were fed.

PointGrey Firefly cameras were used to record the video of the motion. For the experiment, the legs of the Felis Robot were reconfigured for both SLP and ELS configurations. A visible sign was attached to the foot to track its motion from its initial position. An open-loop controller was established using Arduino MEGA Board which gave actuation commands to the Knee Servo Motors. The angular sweep is of 100°.

Fig. 15, Fig. 16 and Fig. 17 compare the Displacement, Velocity and Acceleration Plots of both types of mechanisms along with their X and Y Components. The Dotted Line in all cases represents the SLP mechanism whereas the solid lines represent the ELS mechanism. It can be clearly seen that the ELS mechanism has an increased displacement in terms of cartesian coordinates as compared to an ELS mechanism for the same knee angle displacement in the joint space. Same can be said about the joint velocities and accelerations. This means that it is possible to reach

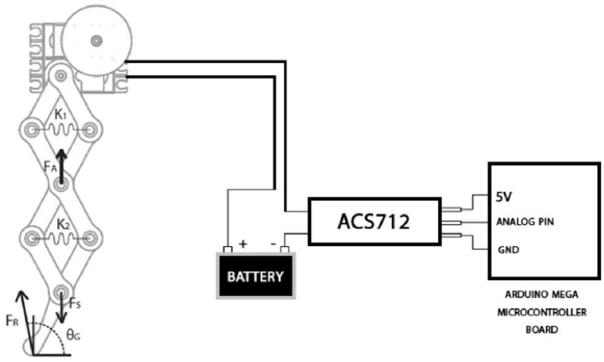

FIGURE 18. Current Measurement Setup of the two Mechanisms (only ELS Mechanism shown).

via points in the trajectory of a servo motor driven leg faster using the ELS technique in contrast to the SLP technique. This makes the ELS mechanism more agile than the SLP Mechanism.

2) COMPARATIVE POWER CONSUMPTION EXPERIMENT

In order to find out the power consumption of both of the mechanisms, the following equation may be considered which equates Electrical Power P_E to Mechanical Power P_M:

$$P_E = P_M \tag{14}$$

$$VI = \tau v \tag{15}$$

$$I \propto \tau \tag{16}$$

where I is the current, τ is the motor torque, V is the Voltage and v is the motor velocity. Although it is a simplification, we can provide similar motor velocities and keep the motor voltage as constant to find out the effect of current on torque. Factors that drastically change the dependencies of torque on current can mostly be resolved if the same motor is used for testing both SLP and ELS mechanisms. In any case, this equation can tell us about the scaling of torque with current for both the mechanisms. Hence if we measure the current, we can get an idea of the torques required by the ELS and the SLP mechanisms.

The experimental setup for measuring torques of the ELS and SLP Mechanisms is shown in Fig. 18.

Current Sensor ACS712 was used in series with the power going to the motor and Power Source to measure the current. The ACS712 sent the Data to the Arduino MEGA board at its analog channel which communicated serially with a logging computer. The results of the experimentation for the SLP mechanism are shown in Fig. 19 while those of the ELS Mechanism are shown in Fig. 20 for consecutive oscillatory motions.

As it can be seen in Fig. 19 and Fig. 20, the average peak current of ELS is almost twice that of SLP. This is the trade-off for the comparatively high speed motion of the ELS mechanism.

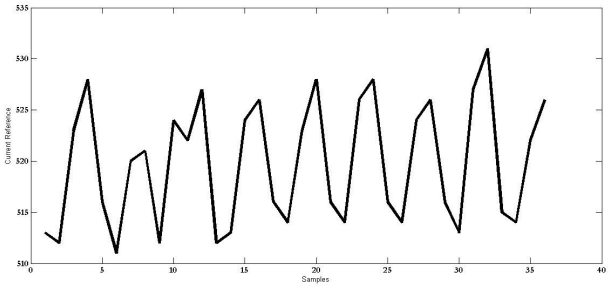

FIGURE 19. Current Consumption (mA) of the SLP Mechanism.

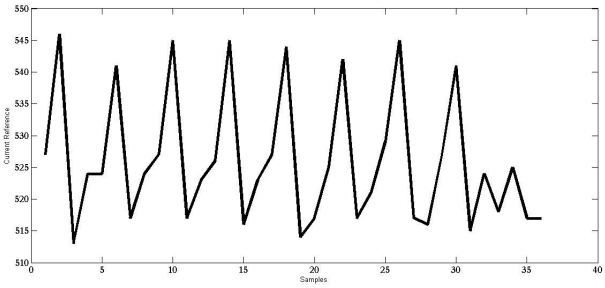

FIGURE 20. Current Consumption (mA) of the ELS Mechanism.

3) POWER CONSUMPTION AT DIFFERENT FREQUENCIES

The power consumed by the mechanism during the entire gait cycle at different frequencies can be analyzed by generating the power-trajectory for the extension/retraction actuator. Only the extension and retraction phases of the gait cycle are of interest for power analysis, because during the stance phase the actuator is decoupled from the mechanism. The servo motor system operates at a constant voltage of 6V and hence the electrical power consumed by the mechanism is proportional to current. Recall that since current is generally proportional to the torque generated by theactuator, so from Eq. 16 it follows:

$$P_E = VI \tag{17}$$

$$\tau = K_\tau I \tag{18}$$

$$I \propto \tau \tag{19}$$

And since V and Kτ are constants in case of a servo motor, so we have

$$\mathrm{P_E} \propto \mathrm{I} \propto \tau \tag{20}$$

Hence generating a current trajectory gives us the shape of both power and torque trajectories. The experimental setup utilized to record the instantaneous current flowing through the servo motor is shown in Fig. 21.

A fifth order Butterworth filter was used with a cutoff frequency of 106 Hz as an anti-aliasing low pass filter. The Arduino Mega 2560 Board samples the filtered current trajectory at 500 Hz and transmits the current values serially to a recording PC.

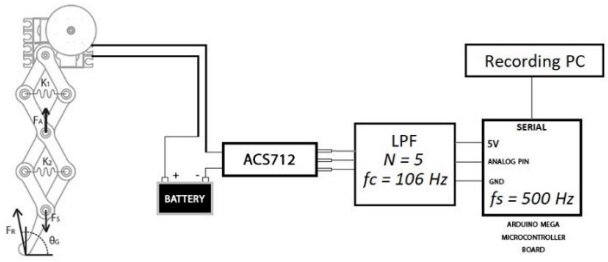

FIGURE 21. Experimental Setup for recording Instantaneous Current. LPF order = 5 and cutoff frequency = 106 Hz.

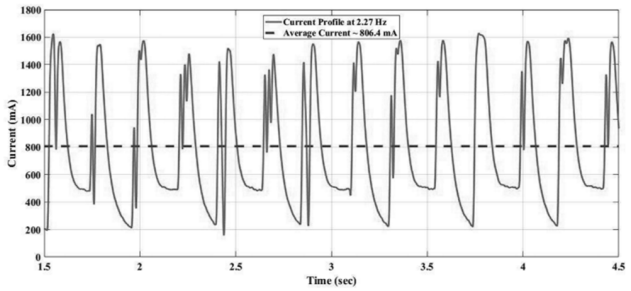

FIGURE 22. Current Trend at 0.5Hz (Solid Line), Average Current 172.6 mA (Dashed Line).

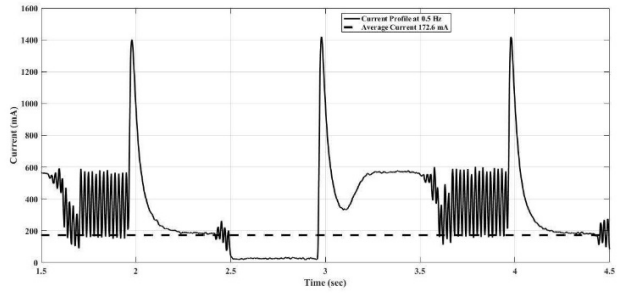

FIGURE 23. Current Trend at 2.27 Hz (Solid Line), Average Current 806.4 mA (Dashed Line).

Fig. 22 shows the current profile for the servo motor at 0.5 Hz of operation and Fig. 23 shows the current profile for the servo motor at 2.27 Hz. As is expected, the power consumption of the servo motor increases as the frequency of operation increases.

4) DISCUSSION

From the above experiments it is quite visible that although the ELS mechanism consumes more current (almost twice) than the SLP mechanism, it delivers higher displacement and velocity in the Cartesian space (almost twice) for the same variations in the actuator space. This is an engineering trade-off and in the design of the legs of the quadruped robots, the high torque requirement is not as impactful due to the unilateral loading of the tendon actuators, however the high-speed response of the ELS mechanism is very impactful and may result in the design of even further high-speed

TABLE 2. Comparison of SLP, Geared SLP and ELS Mechanisms.

Property	SLP	Geared SLP	ELS
Overturning moment	Lowest	High	Low
Stepping frequency	Low	High	High
Max. leg collision region	Large	Large	Small
Energy losses	Friction	Friction/Backlash	Friction
Diameter of knee actuator pulley	Large	Small	Small
Mass distribution modularity	No	No	Yes

dynamic robots. Table 2 shows a comparative summary of the properties of SLP, geared SLP and ELS mechanisms.

Certain important conclusions can be drawn from the stepping frequency experiment. Both the frequencies 0.5 Hz and 2.27 Hz depict an initial surge in current when the leg is being retracted as more power is drawn and a significant decrease in current when the leg is being extended as considerably less power is drawn. The torque generated by the motor is higher during retraction and lower during extension phases. This is expected because during the retraction phase the motor drives the mechanism against gravity and stores elastic potential energy in the elastic element. The same stored elastic energy is released during the extension motion of the mechanism assisted by gravity.

Higher frequencies of operation can be achieved using servo motors at the cost of increased power. The same was observed in the experiments as well.

The experiment in section 6.3 was conducted at 0.5 Hz and 2 Hz with the full range of actuator angular sweep. If the operation frequency is to be increased even more than the limit of 2.5 Hz the range of angular sweep of the actuator must be decreased. This reduced sweep may be insufficient to lift the foot off the ground using SLP mechanisms.

The ELS Mechanism amplifies this small input sweep into a sufficiently large output sweep enabling higher walking frequencies. However, this comes at the cost of higher actuator torque (increased loading). In the experiments that were performed, these high power requirements were within the actuators power limits. This provides a useful engineering trade-off. The average current flowing through the servo motor at 0.5 Hz stepping frequency is 172.6 mA whereas the average current flowing through the servo motor at 2.27 Hz stepping frequency is 806.4 mA.

The Scissors mechanism appears to operate in a similar fashion to a gear transmission in that it trades off torque for higher speeds. However, there are certain advantages of using a scissors transmission mechanism in the proposed scenario. First of all, as gears are generally attached closer to the actuator, the entire Center of Mass (CoM) of the robot is located higher from the ground than the Scissors Mechanism. This would result in higher overturning moments in the geared legs as compared to the ELS Leg during stance (when the foot is planted on the ground). A higher overturning moment affects controllability and stability of a walking robot and is therefore less desirable.

An interesting notion derived from the above argument is that of the emergence of reconfiguration and modularity. It is possible to derive a hybrid transmission mechanism for leg designs that has a gearing stage near the actuator and a scissors transmission in its leg mechanism. This may be helpful in controlling a leg's mass distribution and designing robots that need to vary their leg's output power characteristics, at runtime, based on terrain types.

IV. CONCLUSION

From the above discussion we conclude that the Elastically Loaded Scissors (ELS) Mechanism offers more agile motion due to the possibility of proximal actuation of the knee joint as compared to an Spring Loaded Pantograph (SLP) Mechanism. We have carried out the Kinematics and Elasticity Incorporation Studies on this mechanism and a discussion on workspace variations is also carried out. We have designed a reconfigurable quadruped robot 'Felis' and performed foot motion tracking and motor current consumption experiments on the ELS and SLP configurations. We have concluded that for the two possible configurations in case of Felis, the ELS mechanism amplifies the motion and the torque requirement twice as high as that of the SLP. This however can be made to affect the robot only while unilaterally retracting the leg in the flight phase due to the tendon actuation method while capitalizing on the high speed motion of the foot.

Regarding novelty of the proposed mechanism, the overturning moment of the traditional SLP mechanism is high during the stance phase due to the requirement of a heavier pulley near the shoulders. Similarly, another disadvantage of the SLP mechanism is that it saturates the actuator at lower velocity, for which gears may be required to increase the motor frequency which further increase the overturning moment. Furthermore, when fully collapsed the SLP and geared SLP legs take up more space lateral to the direction of full leg extension axis, which may cause the leg to collide with the ground and hence affect the workable workspace of the leg. As a novelty, our proposed mechanism compensates for these drawbacks.

There are many possible future trajectories for this project. The immediately next task appears to be the design of a stable and simple gait pattern for the locomotion of 'Felis' Robot. A detailed dynamic analysis for optimal control is the subject of ongoing research. We plan to share results on design and control optimization in the future work. We would also like to incorporate servo actuation in the coronal plane to assist the quadruped robot in turning. This could help in a multitude of research topics such as motion planning and even Human Robot Interaction. Mechanically, scaling this mechanism up for applications in larger sized quadruped robots along with the incorporation of a spine is also expected to be performed in the future. Design optimization of the parameters of the Felis robot are also proposed.

APPENDIX: INVERSE KINEMATICS DERIVATION

Inverse Kinematics (or IK in short) involves computation of joint variables that are required by a robot to achieve end effector positions in the task space. These equations are generally non-linear and complex. Additionally, multiple possible solutions may exist to achieve a single position of the end effector in the task-space space.

In some cases, it is impossible to find a closed form analytical solution for finding the inverse kinematics. The problem becomes more involved in the case of closed-linkage mechanisms such as the one proposed in this work. As mentioned earlier in the text, utilizing the parallel nature of linkages, the dimensionality is reduced to the point that the proposed parallel mechanism can be solved as a constrained 3R serial linkage. We use this assumption to calculate the inverse kinematics of the 3R mechanism. The reader is requested to refer to fig. 3 in the text. The forward kinematic equations are rewritten for the 3R case here:

$$x = -l_1 \cos(\theta_1) + l_2 \cos(\theta_1+\theta_2) - l_3 \cos(\theta_1+\theta_2+\theta_3) \quad \text{(i)}$$

$$x = l_1 \sin(\theta_1) - l_2 \sin(\theta_1+\theta_2) + l_3 \sin(\theta_1+\theta_2+\theta_3) \quad \text{(ii)}$$

$$\varphi = \theta_1 + \theta_2 + \theta_3 \quad \text{(iii)}$$

where x and y are the planar coordinates of the foot and φ is the pose of the foot. Adding the parallel linkages constraint we can get value of θ_3:

$$\theta_3 = 2\pi - \theta_2 = -\theta_2 \quad \text{(iv)}$$

Substituting (iv) in (i),(ii) and (iii) we get the equations (21),(22) and (23) mentioned earlier in the text. We hence get value of θ_1

$$x = l_2 \cos(\theta_1+\theta_2) - (l_1+l_3)\cos(\theta_1) \quad (21)$$

$$y = (l_1+l_3)\sin(\theta_1) - l_2 \sin(\theta_1+\theta_2) \quad (22)$$

$$\varphi = \theta_1 \quad (23)$$

Substituting (23) in (21) and (22):

$$x = l_2 \cos(\varphi+\theta_2) - (l_1+l_3)\cos(\varphi) \quad \text{(v)}$$

$$y = (l_1+l_3)\sin(\varphi) - l_2 \sin(\varphi+\theta_2) \quad \text{(vi)}$$

Assume that $\chi = x + (l_1+l_3)\cos(\varphi)$ and $\Upsilon = y - (l_1+l_3)\sin(\varphi)$. Re-writing and rearranging the equations (v) and (vi) yields:

$$\chi = l_2 \cos(\varphi+\theta_2) \quad \text{(vii)}$$

$$\Upsilon = -l_2 \sin(\varphi+\theta_2) \quad \text{(viii)}$$

By dividing equation (viii) by equation (vii) we get a single equation as follows:

$$-\frac{\Upsilon}{\chi} = \tan(\varphi+\theta_2) \quad \text{(ix)}$$

Taking arctan of both sides function on both sides we can retain quadrant information. This yields value of θ_2:

$$\theta_2 = \arctan\left[\frac{y-(l_1+l_3)\sin(\varphi)}{l_2}, \frac{x-(l_1+l_3)\cos(\varphi)}{l_2}\right] - \varphi \quad \text{(x)}$$

Hence equations (iv), (23) and (x) give the inverse kinematics of the robotic leg. Given that there are only 2 independent degrees of freedom and due to the angular constraints enforced by the mechanism itself, it is possible to achieve unique solutions for the foot placement inside the workspace of the robot.

REFERENCES

[1] Y. Washizuka, T. Oshima, K. Koyanagi, and T. Motoyoshi, "The development of a mechanical quadruped robot with animal-like muscle arrangement," in *Proc. IEEE/SICE Int. Symp. Syst. Integr. (SII)*, Dec. 2012, pp. 260–264.
[2] A. Rosendo, S. Nakatsu, K. Narioka, and K. Hosoda, "Pneupard: A biomimetic musculoskeletal approach for a feline-inspired quadruped robot," in *Proc. IEEE/RSJ Int. Conf. Intell. Robots Syst.*, Nov. 2013, pp. 1452–1457.
[3] R. Blickhan, "The spring-mass model for running and hopping," *J. Biomech.*, vol. 22, nos. 11–12, pp. 1217–1227, Jan. 1989.
[4] H.-K. Shin and B. K. Kim, "Energy-efficient gait planning and control for biped robots utilizing the allowable ZMP region," *IEEE Trans. Robot.*, vol. 30, no. 4, pp. 986–993, Aug. 2014.
[5] S. Faraji and A. J. Ijspeert, "3LP: A linear 3D-walking model including torso and swing dynamics," *Int. J. Robot. Res.*, vol. 36, no. 4, pp. 436–455, Apr. 2017.
[6] F. Asano and Y. Zheng, "High-speed and energy-efficient collisionless walking of underactuated rimless wheel," *Artif. Life Robot.*, vol. 23, no. 4, pp. 523–531, Dec. 2018.
[7] R. M. Alexander, "Walking made simple," *Science*, vol. 308, no. 5718, pp. 58–59, 2005.
[8] M. H. Raibert, H. B. Brown, Jr., M. Chepponis, J. Koechling, and J. Hodgins, "Dynamically stable legged locomotion," Leg Lab. Artif. Intell. Lab., Massachusetts Inst. Technol., Cambridge, MA, USA, Tech. Rep. LL-6, 1989.
[9] I. Poulakakis, J. A. Smith, and M. Buehler, "Modeling and experiments of untethered quadrupedal running with a bounding gait: The scout II robot," *Int. J. Robot. Res.*, vol. 24, no. 4, pp. 239–256, Apr. 2005.
[10] M. Raibert, K. Blankespoor, G. Nelson, R. Playter, and T. Team, "Bigdog, the rough-terrain quadruped robot," in *Proc. 17th World Congr.*, vol. 17, 2008, pp. 10822–10825.
[11] M. Hutter, C. Gehring, M. Bloesch, M. A. Hoepflinger, C. D. Remy, and R. Siegwart, "Starleth: A compliant quadrupedal robot for fast, efficient, and versatile locomotion," in *Proc. 15th Int. Conf. Climbing Walking Robot-CLAWAR*, 2012, pp. 483–490.
[12] J. A. Grimes and J. W. Hurst, "The design of atrias 1.0 a unique monopod, hopping robot," in *Proc. Int. Conf. Climbing Walking Robots Support Technol. Mobile Mach.*, 2012, pp. 548–554.
[13] G. Nelson, A. Saunders, and R. Playter, "The PETMAN and atlas robots at Boston dynamics," in *Humanoid Robotics: A Reference*, A. Goswami and P. Vadakkepat, Eds. Dordrecht, The Netherlands: Springer, 2019. [Online]. Available: http://doi-org-443.webvpn.fjmu.edu.cn/10.1007/978-94-007-6046-2_15
[14] G. Zhang, X. Rong, C. Hui, Y. Li, and B. Li, "Torso motion control and toe trajectory generation of a trotting quadruped robot based on virtual model control," *Adv. Robot.*, vol. 30, no. 4, pp. 284–297, Feb. 2016.
[15] G. Secer and U. Saranli, "Control of planar spring-mass running through virtual tuning of radial leg damping," *IEEE Trans. Robot.*, vol. 34, no. 5, pp. 1370–1383, Oct. 2018.
[16] E. R. Westervelt, J. W. Grizzle, C. Chevallereau, J. H. Choi, and B. Morris, *Feedback Control of Dynamic Bipedal Robot Locomotion*. Boca Raton, FL, USA: CRC Press, 2018.
[17] A. C. Hildebrandt, R. Wittmann, F. Sygulla, D. Wahrmann, D. Rixen, and T. Buschmann, "Versatile and robust bipedal walking in unknown environments: Real-time collision avoidance and disturbance rejection," *Auto. Robots*, vol. 48, no. 8, pp. 1957–1976, 2019.
[18] P. Zaytsev, W. Wolfslag, and A. Ruina, "The boundaries of walking stability: Viability and controllability of simple models," *IEEE Trans. Robot.*, vol. 34, no. 2, pp. 336–352, Apr. 2018.
[19] J. Shao, D. Ren, and B. Gao, "Recent advances on gait control strategies for hydraulic quadruped robot," *Recent Patents Mech. Eng.*, vol. 11, no. 1, pp. 15–23, Apr. 2018.
[20] A. Seyfarth, H. Geyer, S. Lipfert, J. Rummel, Y. Blum, M. Maus, and D. Maykranz, "Whole-body mechanics," in *Understanding Mammalian Locomotion*. Hoboken, NJ, USA: Wiley, 2016, pp. 173–191, doi: 10.1002/9781119113713.ch7.

[21] C. Hubicki, A. Abate, P. Clary, S. Rezazadeh, M. Jones, A. Peekema, J. Van Why, R. Domres, A. Wu, W. Martin, H. Geyer, and J. Hurst, "Walking and running with passive compliance: Lessons from engineering: A live demonstration of the ATRIAS biped," *IEEE Robot. Autom. Mag.*, vol. 25, no. 3, pp. 23–39, Sep. 2018.

[22] J. G. D. Karssen, M. Haberland, M. Wisse, and S. Kim, "The effects of swing-leg retraction on running performance: Analysis, simulation, and experiment," *Robotica*, vol. 33, no. 10, pp. 2137–2155, Dec. 2015.

[23] P. A. Bhounsule and A. Zamani, "Stable bipedal walking with a swing-leg protraction strategy," *J. Biomech.*, vol. 51, pp. 123–127, Jan. 2017.

[24] H. R. Vejdani, Y. Blum, M. A. Daley, and J. W. Hurst, "Bio-inspired swing leg control for spring-mass robots running on ground with unexpected height disturbance," *Bioinspiration Biomimetics*, vol. 8, no. 4, Oct. 2013, Art. no. 046006.

[25] J. Duysens and A. Forner-Cordero, "A controller perspective on biological gait control: Reflexes and central pattern generators," *Annu. Rev. Control*, vol. 48, pp. 392–400, Jan. 2019.

[26] A. J. Ijspeert, "Decoding the neural mechanisms underlying locomotion using mathematical models and bio-inspired robots: From lamprey to human locomotion," in *Robotics Research*. Cham, Switzerland: Springer, 2018, pp. 177–186.

[27] J. E. Denham, T. Ranner, and N. Cohen, "Intrinsic and extrinsic modulation of C. Elegans locomotion," *Neuroscience*, May 2018, doi: 10.1101/312132.

[28] F. Dzeladini, N. Ait-Bouziad, and A. Ijspeert, "CPG-based control of humanoid robot locomotion," in *Humanoid Robotics: A Reference*, A. Goswami and P. Vadakkepat, Eds. Dordrecht, The Netherlands: Springer, 2017, doi: 10.1007/978-94-007-7194-9_49-1.

[29] S. Pouya, M. Khodabakhsh, A. Spröwitz, and A. Ijspeert, "Spinal joint compliance and actuation in a simulated bounding quadruped robot," *Auto. Robots*, vol. 41, no. 2, pp. 437–452, Feb. 2017.

[30] Y. Zhong, R. Wang, H. Feng, and Y. Chen, "Analysis and research of quadruped robot's legs: A comprehensive review," *Int. J. Adv. Robotic Syst.*, vol. 16, no. 3, 2019, Art. no. 1729881419844148.

[31] H. Witte, R. Hackert, W. Ilg, J. Biltzinger, N. Schilling, F. Biedermann, M. Jergas, H. Preuschoft, and M. Fischer, "Quadrupedal mammals as paragons for walking machines," in *Proc. Int. Symp. Adapt. Motion Animals Mach. (AMAM)*, Montreal, QC, Canada, 2000, pp. 1–6.

[32] A. Spröwitz, A. Tuleu, M. Vespignani, M. Ajallooeian, E. Badri, and A. J. Ijspeert, "Towards dynamic trot gait locomotion: Design, control, and experiments with cheetah-cub, a compliant quadruped robot," *Int. J. Robot. Res.*, vol. 32, no. 8, pp. 932–950, Jul. 2013.

[33] F. Zhang, X. Yuan, and J. Chen, "Mechanical analysis of scissor transmission mechanism considering friction," in *Applied Mechanics and Materials*, vol. 419, Zurich Switzerland: Trans Tech Publ, 2013, pp. 74–80.

[34] D. Xi and F. Gao, "Type synthesis of walking robot legs," *Chin. J. Mech. Eng.*, vol. 31, no. 1, Dec. 2018.

[35] J. Pratt, C.-M. Chew, A. Torres, P. Dilworth, and G. Pratt, "Virtual model control: An intuitive approach for bipedal locomotion," *Int. J. Robot. Res.*, vol. 20, no. 2, pp. 129–143, Feb. 2001.

[36] Z. Qaiser, L. Kang, and S. Johnson, "Design of a bioinspired tunable stiffness robotic foot," *Mechanism Mach. Theory*, vol. 110, pp. 1–15, Apr. 2017.

[37] M. D. Christie, S. Sun, D. H. Ning, H. Du, S. W. Zhang, and W. H. Li, "A highly stiffness-adjustable robot leg for enhancing locomotive performance," *Mech. Syst. Signal Process.*, vol. 126, pp. 458–468, Jul. 2019.

[38] X. Chen, F. Gao, C. Qi, and X. Zhao, "Spring parameters design to increase the loading capability of a hydraulic quadruped robot," in *Proc. Int. Conf. Adv. Mech. Syst.*, Sep. 2013, pp. 535–540.

[39] M. Vukobratović and B. Borovac, "Zero-moment point—Thirty five years of its life," *Int. J. Humanoid Robot.*, vol. 01, no. 1, pp. 157–173, Mar. 2004.

[40] D. Brown, "Tracker video analysis and modeling tool," Tech. Rep., Aug. 2016.

[41] A. T. Spröwitz, A. Tuleu, M. Ajallooeian, M. Vespignani, R. Möckel, P. Eckert, M. D'Haene, J. Degrave, A. Nordmann, B. Schrauwen, J. Steil, and A. J. Ijspeert, "Oncilla robot: A versatile open-source quadruped research robot with compliant pantograph legs," *Frontiers Robot. AI*, vol. 5, p. 67, Jun. 2018.

[42] S. Rutishauser, A. Sprowitz, L. Righetti, and A. J. Ijspeert, "Passive compliant quadruped robot using central pattern generators for locomotion control," in *Proc. 2nd IEEE RAS EMBS Int. Conf. Biomed. Robot. Biomechtron.*, Oct. 2008, pp. 710–715.

[43] *2019 SOLIDWORKS Help—Introduction to Motion Studies*. Accessed: Nov. 16, 2020. [Online]. Available: http://help.solidworks.com/2019/English/SolidWorks/motionstudies/c_introduction_to_motion_studies.htm

MUHAMMAD HAMZA ASIF NIZAMI (Member, IEEE) received the master's degree from the National University of Sciences and Technology (NUST), Pakistan, in 2016. He is currently a Lecturer with the Department of Robotics and Intelligent Machine Engineering, NUST. His current interests include robot dynamics, legged locomotion, and machine learning.

ZAID AHSAN SHAH received the master's degree from the National University of Sciences and Technology (NUST), Pakistan, in 2017. He is currently a Research Engineer with the Department of Robotics and Intelligent Machine Engineering, NUST. His current research interests include humanoid robots and robot control.

YASAR AYAZ (Senior Member, IEEE) received the Ph.D. degree in mechatronics engineering from Tohoku University, Japan. He is currently an Associate Professor with the Department of Robotics and Intelligent Machine Engineering, National University of Sciences and Technology (NUST), Pakistan. He is also a specially-appointed Associate Professor with the Department of Bioengineering and Robotics, Graduate School of Engineering, Tohoku University, Sendai, Miyagi. His research interests include human–machine interaction and humanoids.

MUHAMMAD JAWAD KHAN (Member, IEEE) received the Ph.D. degree from Pusan National University. He is currently an Assistant Professor with the Department of Robotics and Intelligent Machine Engineering, National University of Sciences and Technology (NUST), Pakistan. His current research interests include machine learning, brain–computer interfacing, bio-inspired robotics, and human–brain interface.

SARA ALI (Member, IEEE) received the Ph.D. degree in robotics and intelligent machine engineering with specialization in human–robot interaction. She is currently an Assistant Professor with the School of Mechanical and Manufacturing Engineering, National University of Sciences and Technology (NUST), Pakistan. Her research interest includes human–robot interaction and human–machine interaction.

MUHAMMAD NAVEED (Member, IEEE) received the Ph.D. degree in robotics from the Institut National des Sciences Appliques, France. He is currently an Assistant Professor with the National University of Sciences and Technology, Islamabad. His research interests include robot motion and state estimation.

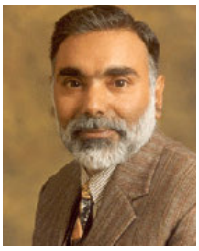

KHALID AKHTAR is a Mechanical Engineer from UET Lahore, with Masters from Cranfield University, U.K. and Doctorate in Industrial Engineering & Management from AIT Bangkok, Thailand. He has fifteen years of field experience in Precision manufacturing. He also has more than 15 years of teaching experience in renowned institutions like GIKI & Bahria University, where he headed the Curriculum Development & Quality Assurance Cell prior to joining NUST. More recently, he was responsible for the development and running of both Masters & Bachelors programs being offered by the School of Mechanical & Manufacturing Engineering at H-12 campus.

DARREN DANCEY received the Ph.D. degree in artificial neural networks. His Ph.D. research was on artificial intelligence. In recent years, he has concentrated on creating collaborations and knowledge exchange between universities and industry with a focus on the SME sector. He is currently the Head of the Department of Computing and Mathematics, Manchester Metropolitan University. He has led several large projects funded by Innovate UK, the Digital R&D Fund for the Arts, and the European Research Council. He is on the organizing committee for the Manchester Raspberry Pi Jam and sits on the BCS Manchester Branch Committee. He has recently taught courses in data structures and algorithms, comparative programming languages, and applied courses such as website development and mobile application development. His teaching interests center on software development.

RAHEEL NAWAZ (Member, IEEE) was an Army Officer. He served in various senior leadership positions in the private Higher and Further Education sector, before becoming a full-time academic. He is currently the Director of digital & technology solutions and a Reader in analytics and applied AI with Manchester Metropolitan University (MMU). He also holds an adjunct and honorary positions with several research organizations in U.K., Middle East, and South Asia. He regularly makes media appearances and speaks on a range of topics, especially artificial intelligence and higher education.